Interplay between structure and magnetism in Ho_xPr_{1-x} alloys. I. Neutron scattering

J. P. Goff* and C. Bryn-Jacobsen
Oxford Physics, Clarendon Laboratory, Oxford OX1 3PU, United Kingdom

D. F. McMorrow
Department of Solid State Physics, Risø National Laboratory, Roskilde DK-4000, Denmark

G. J. McIntyre
Institut Laue-Langevin, 156X, 38042 Grenoble Cedex, France

J. A. Simpson, R. C. C. Ward, and M. R. Wells
Oxford Physics, Clarendon Laboratory, Oxford OX1 3PU, United Kingdom

(Received 24 July 1997)

The structural and the magnetic ordering in thin-film Ho_xPr_{1-x} alloys have been studied using neutron- and x-ray-diffraction techniques. As the concentration of Ho decreases the alloys adopt hexagonal-close-packed (hcp), Sm, and double hexagonal-close-packed (dhcp) crystal structures. The results show enhanced occupation of the cubic sites by Pr in the Sm and dhcp phases. The magnetic behavior is found to be very different in the three crystalline phases. The hcp samples form basal-plane spirals and the alloys with the Sm structure form a commensurate magnetic structure with the same periodicity as the magnetic order on the hexagonal sites in Sm metal, but the moments are confined to the basal plane. At low temperatures both Ho and Pr are found to adopt their full saturation moments in these phases. A Pr thin film is found to order with a similar magnetic structure to bulk Pr. However, no long-range magnetic order is observed in the dhcp alloys down to a temperature $T\sim 23$ mK, suggesting that Ho and Pr have singlet ground states and that the ordering due to the hyperfine interaction is suppressed. The results are discussed in terms of mean-field theory and the concentration dependence of the Néel temperature is found to be anomalous. [S0163-1829(98)05809-3]

I. INTRODUCTION

Previously there have been numerous studies of the properties of rare-earth alloys produced using bulk techniques. However, molecular-beam epitaxy (MBE) now enables the production of precise compositions of alloys that are generally superior in homogeneity and crystalline quality. Using MBE it is possible to produce random alloy samples because the growth is not under equilibrium conditions and so clustering and concentration gradients are less likely. Single-crystal thin films of Ho_xPr_{1-x} alloys have been grown using MBE and the magnetic structures have been determined using neutron-diffraction techniques. Ho_xPr_{1-x} alloys form solid solutions over the entire composition range, with hexagonal-close-packed (hcp), samarium (Sm), or double hexagonal-close-packed (dhcp) crystal structures, depending on the concentration x. The aim of the experiment was to determine how the magnetic ordering in Ho and Pr is affected by alloying and by the concomitant changes in crystal structure.

Bulk Ho has the hcp crystal structure and orders below $T_N\sim 132$ K in a helical structure with moments confined to the basal plane and the modulation vector of the helix along the hexagonal c axis.[1] The wave vector $\boldsymbol{q}$ is incommensurate at the ordering temperature and decreases with temperature until it locks into a series of commensurate values, associated with the so-called spin-slip structures.[2,3] Below $T\sim 20$ K there is a transition to a cone phase with $\boldsymbol{q}=(1/6)\boldsymbol{c}^*$ and a ferromagnetic component along the $\boldsymbol{c}$ axis. The crystal structure of Pr metal is dhcp and therefore contains sites of approximately cubic and hexagonal local symmetry. The crystal-field interactions are larger than the exchange and both the hexagonal and cubic sites have nonmagnetic singlet ground states. Pr does not exhibit spontaneous long-range magnetic order until it is induced by the hyperfine coupling at $T\sim 45$ mK.[4] However, the hexagonal sites are close to ordering at low temperatures[5] and ordering may be induced by impurities such as Nd,[4] uniaxial stress,[6] or the application of an external magnetic field.[7] When the hexagonal sites order they form a longitudinal incommensurate modulation along $\boldsymbol{a}^*$, with antiferromagnetic coupling between adjacent hexagonal layers.

The magnetic properties of rare-earth alloys in which the crystal structure remains unaltered have been studied extensively.[8,9] Heavy rare-earth elements diluted by Y and Lu have the hcp structure and the $\boldsymbol{c}$ axis modulated antiferromagnetic structures of the rare-earth elements are found to persist in the alloys. In the case of Ho alloys with Y,[10] Lu,[11] and Sc,[12] thin films grown using MBE have been investigated and the magnetic structure is a basal-plane helix. In these systems the concentration dependence of the Néel temperature can be described by the virtual-crystal model, where the peak in the conduction-electron susceptibility varies linearly between that of the pure constituents. The magnetism of Nd_xPr_{1-x} alloys, which form a complete range of solid solutions with the dhcp structure, has also been studied extensively.[4,13–15] The hexagonal sites order with antiferromagnetic coupling between adjacent layers and an incom-

mensurate modulation within the basal plane. All of the above systems may be understood in terms of mean-field theory.

The behavior of Ho_xPr_{1-x} alloys is found to be rather different and this paper describes neutron-scattering studies of the magnetic ordering in this system. Section II gives details of the experimental procedure and this is followed in Sec. III by the results of x-ray- and neutron-diffraction measurements of the crystal structure. Then the main results of the paper, the neutron-diffraction study of the magnetic order, are presented in Sec. IV. The discussion of the results in Sec. V includes a comparison with mean-field calculations and then some conclusions are drawn in Sec. VI. A complementary study of these alloys using resonant x-ray magnetic scattering is described in the following paper.[16]

II. EXPERIMENTAL PROCEDURE

The random Ho_xPr_{1-x} alloys were grown by MBE using the Balzers UMS630 facility at the Clarendon Laboratory. The growth techniques were similar to those developed for Ho_xY_{1-x} alloys.[10] A 1000-Å Nb buffer layer separates the rare-earth elements from the 1-mm-thick sapphire substrate and a 1000-Å Y seed and 250-Å Y cap enclose the alloy. Ho is deposited from a Knudsen effusion cell and Pr from an electron-beam source at a combined rate of 1 Å s^{-1}, controlled to provide the designated concentration x of Ho and an overall thickness of about 14000 Å. The relatively high growth temperature of 870 K was employed to ensure the production of highly uniform alloys. The epitaxial relationships are $\{1\,1\,0\}Al_2O_3 \| \{1\,1\,0\}Nb \| \{0\,0\,1\}Y, Ho_xPr_{1-x}$. The crystal structures were determined using high-resolution triple-crystal diffractometers on a rotating anode x-ray generator at the Clarendon Laboratory.

Neutron-diffraction studies of the structural and magnetic ordering were carried out using the triple-axis spectrometer TAS1, which is situated on a cold neutron source at Risø National Laboratory. Here a fixed incident neutron energy $E_i = 5$ meV was chosen since this gave adequate wave-vector transfer range and resolution while allowing the suppression of higher-order scattering with a beryllium filter. Measurements were performed for all samples using a variable-temperature cryostat over the range 1.8 K to room temperature. Further measurements were performed on samples with the dhcp structure using the diffractometer $D10$ at the Institut Laue-Langevin. Thermal neutrons with a fixed energy $E_i \sim 14.8$ meV were selected and a pyrolitic-graphite filter was used. Energy analysis was again employed to separate the elastic magnetic diffraction from the thin films from the inelastic background. The samples were mounted in a dilution cryostat, which operated with a base temperature $T \sim 23$ mK. Good thermal contact was achieved by clamping the samples with the rare-earth surface in contact with a copper block.

III. CRYSTAL STRUCTURES

The structural order was investigated first using x-ray-diffraction techniques. The mosaic spreads are found to be in the range 0.1°–0.2°, which is typical of rare-earth alloys grown using this technique. The concentrations x were estimated by taking the known Ho thin-film c-axis lattice parameter,[10] the measured Pr lattice parameter, and assuming a linear dependence on x. These values are consistent with the nominal concentrations, but are found to vary with position on the film by as much as 5%. The widths of the Bragg reflections give structural correlation lengths in the range 300–1000 Å, which are considerably smaller than for other MBE-grown thin films, and this indicates a relatively high concentration of stacking faults. The free energies of the different crystalline phases hcp, Sm, and dhcp become comparable near the phase boundaries, so the alloys may contain small metastable regions of different phases.

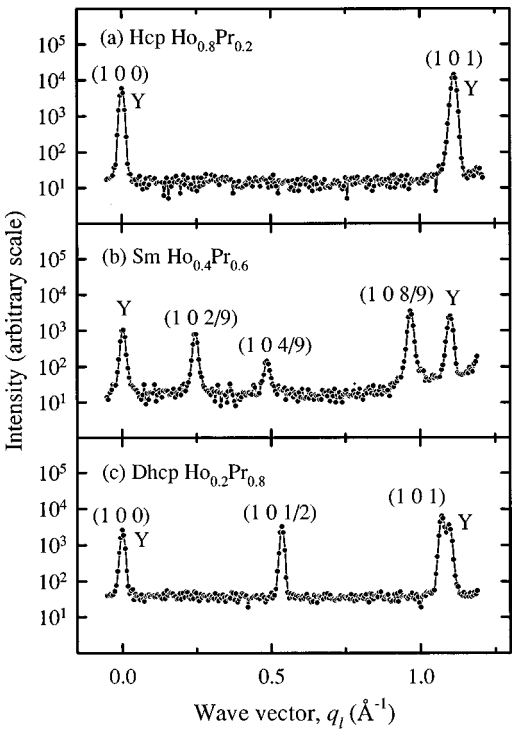

FIG. 1. Neutron-scattering intensity measured in scans of $\boldsymbol{Q}$ along the $[1\,0\,q_l]$ direction for (a) $Ho_{0.8}Pr_{0.2}$ at $T = 140$ K, (b) $Ho_{0.4}Pr_{0.6}$ at $T = 100$ K, and (c) $Ho_{0.2}Pr_{0.8}$ at $T = 120$ K. The peaks are labeled using the hcp reciprocal cell and the crystal structures are (a) hcp, (b) Sm, and (c) dhcp. The Y (1 0 0) and (1 0 1) peaks are also present in each case.

The scattering measured above T_N using neutron diffraction is shown for wave-vector transfer $\boldsymbol{Q}$ along $[1\,0\,q_l]$ in Fig. 1 and $[0\,0\,q_l]$ in Fig. 2. The scattering along $[1\,0\,q_l]$ is determined by the stacking sequence of the hexagonal-close-packed planes, whereas the scattering along $[0\,0\,q_l]$ is not sensitive to the position of the ions within the close-packed planes. The scattering from $Ho_{0.8}Pr_{0.2}$, $Ho_{0.4}Pr_{0.6}$, and $Ho_{0.2}Pr_{0.8}$ alloys is consistent with that expected for the hcp, Sm, and dhcp crystal structures, respectively. In each case the Bragg reflections from hcp Y are also present. The crystal structures derived for each composition are listed in Table I.

The three different crystal structures are expected to give the same scattering along $[0\,0\,q_l]$, labeled (0 0 2) in Fig. 2. However, for dhcp $Ho_{0.2}Pr_{0.8}$ intensity is also observed at $\boldsymbol{Q} = (0\,0\,1)$. Using the much higher-intensity x rays, extra diffraction peaks were also detected along $[0\,0\,q_l]$ for samples with the Sm structure, as shown in Fig. 3. In this case there

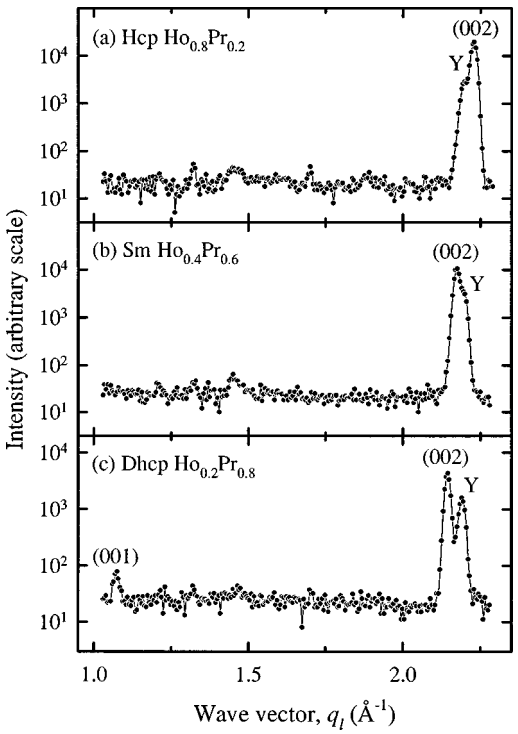

FIG. 2. Neutron-scattering intensity measured in scans of $\boldsymbol{Q}$ along the $[0\,0\,q_l]$ direction for (a) $Ho_{0.8}Pr_{0.2}$ at $T=140$ K, (b) $Ho_{0.4}Pr_{0.6}$ at $T=100$ K, and (c) $Ho_{0.2}Pr_{0.8}$ at $T=120$ K. An extra peak is observed in (c) at $\boldsymbol{Q}=(0\,0\,1)$ in the hcp reciprocal cell.

are unexpected reflections at $q_l=2n\pm2/3$, where n is an integer. The dhcp *ABAC* and Sm *ABABCBCAC* structures comprise cubic and hexagonal sites in the sequences *chch* and *chhchhch*, respectively. Thus the extra peaks for both dhcp and Sm phases would occur if there were different concentrations of Ho and Pr on the two inequivalent sites or if the interplanar spacings between the hexagonal planes d_{hh} and cubic and hexagonal planes d_{hc} were to differ. Figure 4 shows the integrated intensities of the peaks for the $Ho_{0.4}Pr_{0.6}$ alloy after polarization, Lorentz, and form factor corrections. Allowing only the concentrations to vary gives a constant structure factor for the $q_l=2n\pm2/3$ peaks, whereas the strain model predicts that the structure factors vary as Q^2 and therefore the former is more consistent with the experimental data. The best fit of these two models is shown in Fig. 4 and this yields a concentration of Ho on the cubic sites of (12 ± 15)% and a displacement $d_{hc}-d_{hh}\leqslant0.005$ Å. A comparison of the neutron-diffraction intensities at $\boldsymbol{Q}=(001)$ and (002) from $Ho_{0.2}Pr_{0.8}$ also gives a low occupancy of (5 ± 3)% on the cubic sites by Ho. The large departure from the nominal concentrations may arise because the Ho tends to occupy the hexagonal sites that are present in its stable phase.

TABLE I. Summary of the crystal stuctures, Néel temperatures, and magnetic structures of Ho_xPr_{1-x} alloys determined by neutron- and x-ray-diffraction techniques. The results for the Ho thin film are taken from Ref. 10.

Structures and magnetic order in Ho_xPr_{1-x} alloys			
x	Crystal structure	T_N (K)	Magnetic structure
1.0	hcp	131	basal-plane spiral
0.8	hcp	100	basal-plane spiral
0.6	hcp	64	basal-plane spiral
0.5	Sm	40	Sm hexagonal type
0.4	Sm	30	Sm hexagonal type
0.3	dhcp	<0.023	no long-range order
0.2	dhcp	<0.023	no long-range order
0.0	dhcp	0.114	Pr hexagonal type

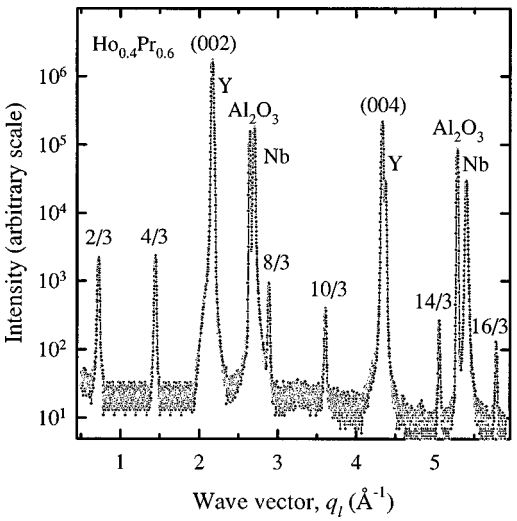

FIG. 3. X-ray-scattering intensity measured in a scan of $\boldsymbol{Q}$ along the $[0\,0\,q_l]$ direction for $Ho_{0.4}Pr_{0.6}$ at room temperature. Extra reflections are observed at $q_l=2n\pm2/3$, where n is an integer (hcp reciprocal cell).

IV. MAGNETIC STRUCTURES

A. hcp phase

The neutron scattering observed from $Ho_{0.8}Pr_{0.2}$ for wave-vector transfers $\boldsymbol{Q}$ along the $[0\,0\,q_l]$ direction is shown in Fig. 5 for (a) $T=40$ K and (b) $T=4$ K. The magnetic peak in Fig. 5(a) is displaced from the structural (0 0 2) reflection

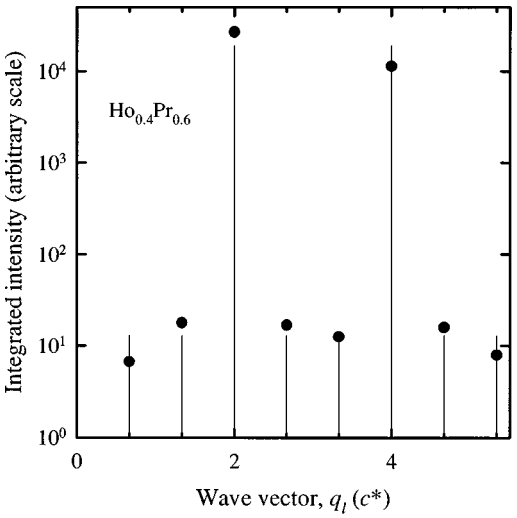

FIG. 4. Observed structure factors (filled circles) and the best fit (solid lines) of a model that allows for different Ho and Pr concentrations on the cubic and hexagonal sites and for strain.

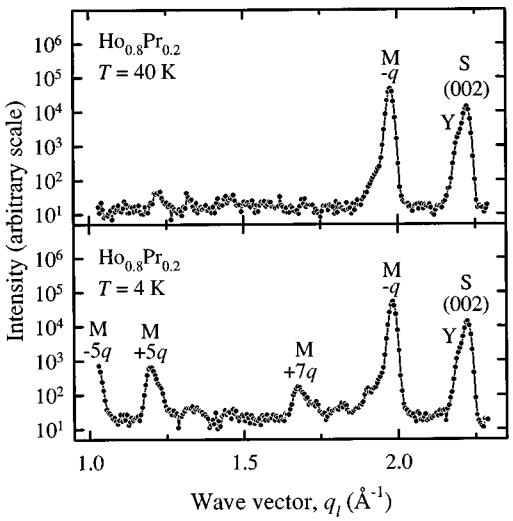

FIG. 5. Neutron-scattering intensity from $Ho_{0.8}Pr_{0.2}$ measured in scans of $\boldsymbol{Q}$ along $[0\ 0\ q_l]$ (a) at $T=40$ K and (b) at $T=4$ K. The structural and magnetic peaks are labeled S and M, respectively. In (b) q is commensurate and fifth and seventh harmonics are observed.

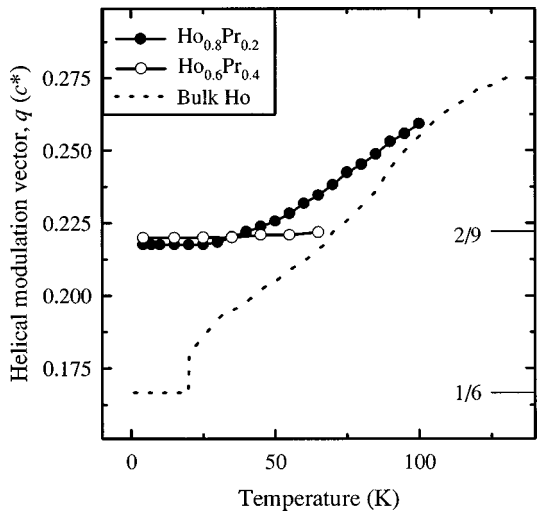

FIG. 7. Temperature dependence of q for hcp Ho_xPr_{1-x} alloys compared with the values for bulk Ho taken from Ref. 2.

by an incommensurate modulation vector $\boldsymbol{q}$. A comparison with the data measured along the $[1\ 0\ q_l]$ direction shows that the results are consistent with a helical magnetic structure with moments confined to the basal planes and the modulation vector in the $\boldsymbol{c}^*$ direction. At lower temperatures $\boldsymbol{q}$ becomes commensurate with the crystal lattice and Fig. 5(b) shows fifth and seventh harmonics from (0 0 2) and the origin.

The Néel temperatures for Ho_xPr_{1-x} are shown as a function of x in Fig. 6. The temperature dependence of the helical modulation vectors for the hcp Ho_xPr_{1-x} alloys are shown in Fig. 7, along with data obtained previously from bulk Ho.[2] Both T_N and $q(T_N)$ are found to decrease with dilution by Pr far more rapidly than has been reported for other nonmagnetic ions such as Y, Lu, or Sc.[10–12] Furthermore, the variation in modulation vector Δq over the full temperature range is smaller for the Ho_xPr_{1-x} alloys. The modulation wave vectors lock in at low temperature to the values $\boldsymbol{q}=0.218(5)$ and 0.221(5) $\boldsymbol{c}^*$ for $Ho_{0.8}Pr_{0.2}$ and $Ho_{0.6}Pr_{0.4}$, respectively. These are, within error, the commensurate value $2/9\boldsymbol{c}^*$, which is associated with the (2,1) spin-slip structure.

The average moment per site has been determined by comparing the intensities of the magnetic $(0\ 0\ 2-q)$ and nuclear (0 0 2) reflections and correcting for basal-plane spiral and hcp structure factors, the magnetic form factor, and the Lorentz factor. The temperature dependence of the magnetic moment measured for $Ho_{0.6}Pr_{0.4}$ is shown in Fig. 8 and the saturation moments measured for each sample composition are listed in Table II. In order to investigate the phase transition the scattering has been measured in detail in the vicinity of T_N. The intensity was fitted to Gaussian profiles obtained in scans of $\boldsymbol{Q}$ in the $[0\ 0\ q_l]$ direction and the intensities and widths are presented in Fig. 9. The integrated intensities [Fig. 9(a)] are found to be approximately proportional to T_N-T over a wide range of temperatures below T_N, but there is a rounding very close to T_N. Figure 9(b)

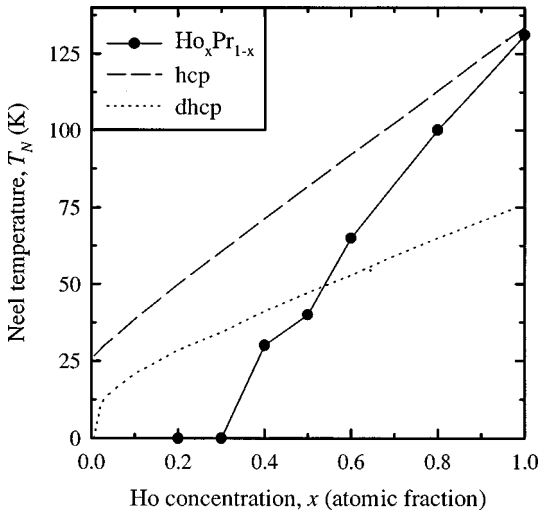

FIG. 6. Dependence of T_N on x for Ho_xPr_{1-x} alloys compared with mean-field calculations, as described in Sec. V.

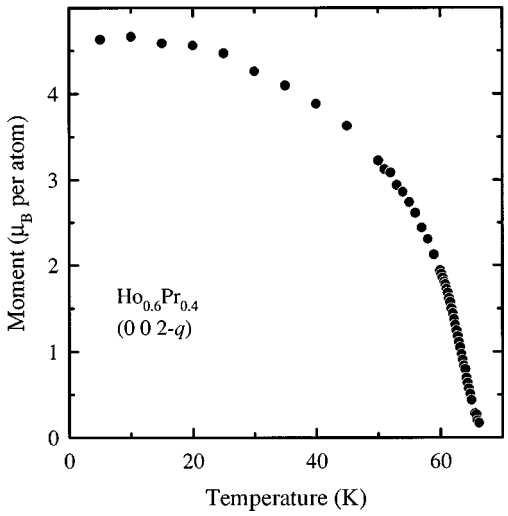

FIG. 8. Temperature dependence of the mean magnetic moment per atom for the $Ho_{0.6}Pr_{0.4}$ alloy determined using the magnetic intensity at $\boldsymbol{Q}=(0\ 0\ 2-q)$.

TABLE II. Experimental saturation moments μ_{expt}^{sat} for Ho_xPr_{1-x} alloys. The theoretical value $\mu_{Ho,Pr}^{sat}$ assumes ordering of Ho and Pr moments and μ_{Ho}^{sat} assumes ordering of Ho only.

x	μ_{expt}^{sat}	$\mu_{Ho,Pr}^{sat}$	μ_{Ho}^{sat}
0.8	8.55	7.36	8
0.6	4.63	4.72	6
0.5	3.17	3.40	5
0.4	2.11	2.08	4

shows that the rounding is accompanied by a broadening of the peak, so that this can be associated with critical scattering. The solid line in Fig. 9(a) shows a least-squares fit of the conventional exponent relationship $I(T)=A(T_N-T)^{2\beta}$, which yields $\beta=0.55(3)$ and $T_N=63.8(2)$ K. Thus the critical exponent is similar to that reported for Ho and Ho_xY_{1-x} thin films.[10]

B. Sm phase

For samples with the Sm crystal structure magnetic peaks were detected at (0 0 5/3), (1 0 1/9), (1 0 5/9), and (1 0 7/9) using the hcp basis for reciprocal space. The ordering wave vectors are independent of temperature and the peak intensities increase steadily with decreasing temperature until saturation occurs. The neutron scattering from $Ho_{0.4}Pr_{0.6}$ at $T=4$ K is shown in Fig. 10 for scans of $\boldsymbol{Q}$ along (a) $[0\,0\,q_l]$ and (b) $[1\,0\,q_l]$. The observed magnetic reflections are consistent with a magnetic structure comprising ferromagnetic hexagonal-close-packed planes in the sequence $0{+}{+}0{-}{-}0{+}{+}0{-}{-}\cdots$ and this is very similar to the magnetic ordering on the hexagonal sites in Sm.[17] However, the strong magnetic intensity for $\boldsymbol{Q}$ along $[0\,0\,q_l]$ [see Fig. 10(a)] suggests that in this case the moments are confined to the basal plane. An extra set of magnetic reflections is observed at low temperature for Sm metal, which is attributed to ordering on the cubic sites. Since these peaks are not observed

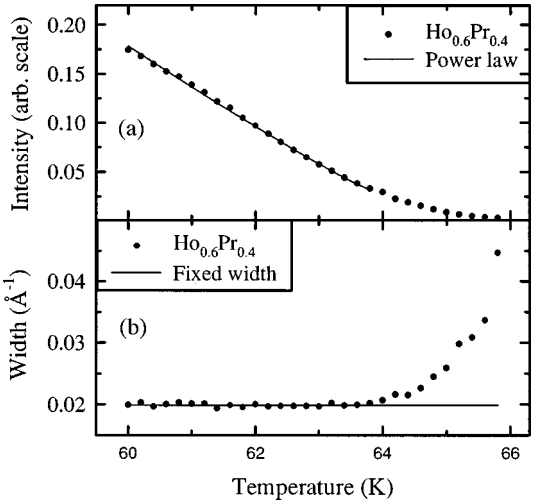

FIG. 9. Temperature dependence of the neutron scattering from $Ho_{0.6}Pr_{0.4}$ at $\boldsymbol{Q}=(0\,0\,2-q)$ showing (a) the integrated intensity and (b) the width in the c direction. The solid line in (a) shows a fit of a power law, which gives $T_N=63.8(2)$ K and $\beta=0.55(3)$. The rounding in (a) correlates with the broadening in (b) and may be attributed to critical scattering.

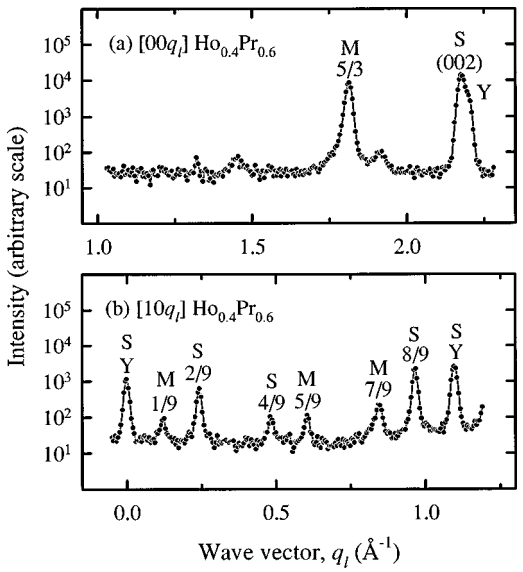

FIG. 10. Neutron-scattering intensity measured in scans of $\boldsymbol{Q}$ along (a) $[0\,0\,q_l]$ and (b) $[1\,0\,q_l]$ for $Ho_{0.4}Pr_{0.6}$ at $T=4$ K. The structural and magnetic peaks are labeled S and M, respectively. The fractions give q_l in units of c^* using the hcp reciprocal cell. The small magnetic peak at $q_l\sim1.913$ Å^{-1} in (a) is attributed to the presence of small hcp regions.

for Ho_xPr_{1-x} alloys it is assumed that only the hexagonal sites order. The proposed magnetic structure is shown in Fig. 11 and the saturation moments determined assuming this structure are listed in Table II. The dependence of T_N on x is shown in Fig. 6.

In the hcp $Ho_{0.6}Pr_{0.4}$ sample a small magnetic peak was detected, which possibly arises from small regions (less than 10%) with the Sm structure. Similarly, all samples with the Sm structure exhibit small magnetic peaks associated with basal-plane spirals from regions with the hcp structure [see Fig. 10(a)]. This is consistent with the metastabilty of phases and concentration gradients inferred from the x-ray-diffraction measurements.

C. dhcp phase

The magnetic scattering observed using $D10$ for $\boldsymbol{Q}\sim(q_h\,0\,3)$ from the Pr thin film at a temperature $T\sim23$ mK is presented in Fig. 12. The temperature dependence of the integrated intensity of this peak, shown as the inset in Fig. 12, confirms that the scattering is magnetic and shows that saturation occurs below $T\sim50$ mK. The Néel temperature deduced from these data is $T_N\sim114(5)$ mK, which is higher than the value quoted for bulk Pr, $T_N\sim45$ mK.[4] The in-plane modulation vector is $q_h=0.126(1)\boldsymbol{a}^*$, compared to $q_h\sim0.128\boldsymbol{a}^*$ for bulk Pr, suggesting that the magnetic structures are similar. The position remains fixed as the temperature varies and is close to the commensurate value $q_h=\frac{1}{8}\boldsymbol{a}^*$. Unlike bulk Pr,[4] the width of the magnetic reflection is resolution limited at all temperatures and no broad component was observed.

Despite exhaustive searches no magnetic diffraction peaks could be detected for the $Ho_{0.2}Pr_{0.8}$ and $Ho_{0.3}Pr_{0.7}$ alloys. A variety of scans of $\boldsymbol{Q}$ were attempted in the $(h0l)$ and (hhl) planes using TAS1 and the $(h0l)$ plane using $D10$, particularly in regions where magnetic peaks have been observed in

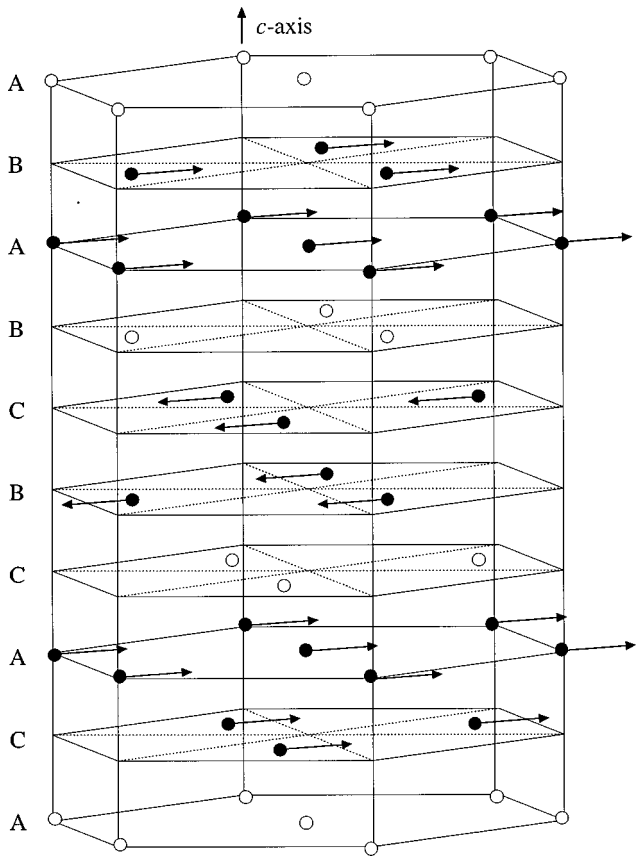

FIG. 11. Proposed magnetic structure for Ho_xPr_{1-x} alloys with the Sm crystal structure. The hexagonal sites are shown as filled circles and the cubic sites as empty circles. The magnetic unit cell contains 18 close-packed planes.

other dhcp rare earth elements. Thus the Ho inhibits magnetic ordering above the lowest temperature $T=23$ mK. Figure 12 compares the scattering observed from the $Ho_{0.2}Pr_{0.8}$ alloy near $\boldsymbol{Q}=(0.126\ 0\ 3/2)$ with the data for thin-film Pr acquired under identical conditions. This shows that, even

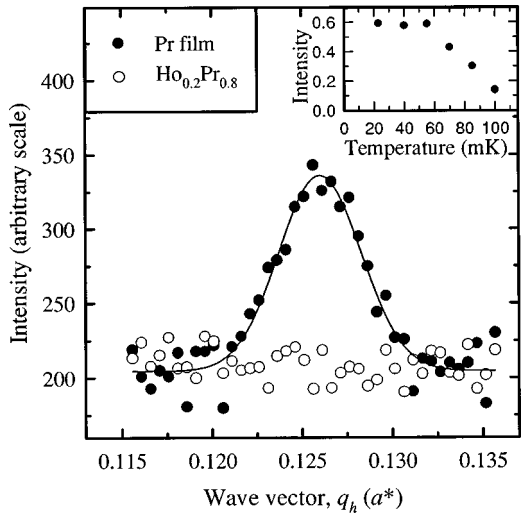

FIG. 12. Neutron-scattering intensity measured in scans of $\boldsymbol{Q}$ along $[q_h\ 0\ 3/2]$ for the Pr thin film and the $Ho_{0.2}Pr_{0.8}$ alloy at $T=23$ mK. The inset shows the temperature dependence of the integrated intensity of the magnetic reflection at $\boldsymbol{Q}=(0.126\ 0\ 3/2)$ for the Pr thin film.

TABLE III. Exchange and crystal-field parameters for the rare-earth ions on hexagonal sites in units of meV.

Ion^{3+}	$J(Q)$	B_2^0	B_4^0	B_6^0	B_6^6
Ho	0.450	0.024	0.0	-9.6×10^{-7}	9.2×10^{-6}
Pr	0.161	0.19	-5.7×10^{-4}	1.0×10^{-4}	-9.6×10^{-4}

though the Pr moments are small, it would have been possible to detect magnetic scattering under these conditions in the thin film alloys. Hence the Pr ordering is suppressed by dilution with Ho.

The magnetic structures and Néel temperatures determined using neutron diffraction are summarized in Table I.

V. DISCUSSION

The magnetic structures of the rare-earth elements depend on the indirect exchange via the conduction electrons, the crystal fields, and the strain.[5] The Néel temperatures and modulation wave vectors are determined primarily by the magnitude and position of a peak in the conduction-electron susceptibility $\chi(\boldsymbol{q})$. This peak is associated with nesting features in the Fermi surface[18] and is therefore very sensitive to any changes in the crystal structure. Furthermore, there are sites of approximately cubic local symmetry in the Sm and dhcp crystal structures, as well as hexagonal sites. Consequently, the magnetism of the Sm and dhcp Ho_xPr_{1-x} alloys is rather different from that of the previously studied hcp alloys.

Assuming that the peak in $\chi(q)$ is determined primarily by crystal structure one might expect the hcp, Sm, and dhcp samples to have magnetic structures with similar modulation wave vectors to Ho, Sm, and Pr, respectively. The hcp samples order in a basal-plane spiral as expected. The samples with the Sm structure adopt a commensurate magnetic structure with the same periodicity as Sm metal. However, unlike the hexagonal sites in Sm metal, the axial anisotropies of Ho and Pr both favor confinement of the moments to the basal plane. Neutron-diffraction studies of single-crystal Tb:La, Tb:Pr, and Tb:Nd show that these rare-earth alloys with the Sm structure exhibit similar magnetic structures.[19] Furthermore, Tb:Pr and Tb:Nd undergo martensitic phase transitions to the hcp structure below $T\sim30$ K and then a ferromagnetic structure similar to pure Tb is observed. It is surprising that the dhcp Ho_xPr_{1-x} alloys do not order, particularly since dhcp Er:Pr (Ref. 20) orders with a magnetic structure which resembles that of Pr.

The exchange and crystal-field parameters for the pure metals are listed in Table III. Since B_2^0 is positive for both ions the Ho_xPr_{1-x} alloys are an easy-planar system. The Ho ions tend to point along $\boldsymbol{a}^*$ and this is the direction favored also by the two-ion anisotropy in Pr. The virtual-crystal approximation for a binary alloy gives spontaneous long-range magnetic order when[5]

$$[x\chi_1^0+(1-x)\gamma^2\chi_2^0]J(Q)=1, \tag{1}$$

where $J(Q)$ is the exchange, χ^0 is the noninteracting single-ion susceptibility, and the indices 1 and 2 refer to the two types of ion. The γ factor is defined by

$$\gamma=(g_2-1)/(g_1-1) \tag{2}$$

and this gives

$$\gamma^2 J_{11}(Q)=\gamma J_{12}(Q)=J_{22}(Q). \tag{3}$$

The fact that γ is negative for Ho_xPr_{1-x} means that Ho and Pr moments are antiparallel, but does not affect the ordering temperature. The results of mean-field calculations of T_N for the Ho_xPr_{1-x} system are compared with the experimental data in Fig. 6.[21] The dashed curve is an extrapolation from the high-temperature model for hcp Ho.[22] The dotted line was determined assuming the model for the magnetic structure on the hexagonal sites of dhcp Pr.[23] This model takes account of the cubic sites by using an effective exchange for the hexagonal sites and this approach should apply to the dhcp alloys if the cubic Ho sites also have a singlet ground state. In the Pr model the two crystal-field level schemes have singlets as ground states and so, neglecting the hyperfine interaction, the dhcp alloys should not order. However, the Ho ions should induce a magnetically ordered state and the virtual-crystal model gives a threshhold Ho concentration $x\sim 0.005$.

The observed Néel temperatures are anomalously low for Ho_xPr_{1-x} alloys, even in the hcp and dhcp phases, where the mean-field calculation should be most reliable. The results will be affected by the different occupancies on the cubic and hexagonal sites, but an enhanced occupation of hexagonal sites by Ho is unlikely to suppress T_N. The crystal-field parameters may differ from the pure values in the environment of the alloy, but not sufficiently to explain the discrepancy between theory and experiment. Another possibility is that the exchange is drastically modified in the Ho_xPr_{1-x} alloys. This is supported by the results for the hcp phase, where the rapid variation of $q(T_N)$ with concentration demonstrates that the Fermi surface is changing. The topology of the Fermi surface depends critically on c/a (Ref. 24) and relatively small changes can have a dramatic effect on $\chi(\boldsymbol{q})$. For Ho_xPr_{1-x} the variation in c/a over the full composition range is about 3% and this is considerably larger than for the other hcp rare-earth alloys[8–12] and may be responsible for the unusual behavior.

The absence of magnetic ordering in the dhcp alloys of Ho_xPr_{1-x} suggests that both the hexagonal and cubic sites of Ho and Pr have singlet ground states in this phase. The exchange interaction in pure Pr is only just insufficient to overcome the crystal-field splitting for the hexagonal sites and induce magnetic ordering.[4] In pure Pr the hyperfine interaction between the nuclear moments and the conduction electrons is sufficient to induce order at $T_N\sim 45$ mK. The nuclear moments are 4.25 and 4.03 μ_n for Pr and Ho, respectively, and therefore, dilution by Ho is not expected to suppress the magnetic ordering in Pr. The behavior is very different for dhcp Er:Pr, where the change in c/a is similar, but the Néel temperature is elevated from the Pr value to $T_N\sim 2.4$ K.[20] This corresponds to an increase of $J(Q)$ in Eq. (1) with Er concentration, in contrast to the decrease produced by the Ho ions in the present dhcp system.

Since γ is negative for Ho_xPr_{1-x} alloys any localized moment on a Pr ion would point in the opposite direction to a Ho moment on the same site. Therefore, if both the Ho and Pr ions fully order

$$\mu^{sat}_{Ho,Pr}=xg_{Ho}S_{Ho}-(1-x)g_{Pr}S_{Pr}, \tag{4}$$

whereas if only the Ho ions order

$$\mu^{sat}_{Ho}=xg_{Ho}S_{Ho}. \tag{5}$$

Here x is the Ho concentration, g is the Landé factor, and S is the angular momentum. Table II compares these expressions for the theoretical saturation moments with the measurements for the hcp and Sm structured Ho_xPr_{1-x} alloys and the results show that the Pr ions are fully ordered in these phases. It is worth noting that it should have been possible to detect any magnetic ordering in the dhcp Ho_xPr_{1-x} alloys even though opposing moments would reduce the magnetic neutron-diffraction intensity. The ordering on the Pr sites may also explain the small variation in modulation vector Δq for the hcp Ho_xPr_{1-x} alloys. The change of wave vector with temperature is associated with the development of magnetic superzone gaps as the ordered moments increase,[25] but the average moment is reduced by the ordering on the Pr sites.

VI. CONCLUSIONS

Ho_xPr_{1-x} forms solid solutions with the hcp, Sm, and dhcp crystal structures. There is a preferred occupancy by Ho of the hexagonal sites of the Sm and dhcp structures. The hcp- and Sm-structured alloys order with magnetic structures similar to those observed in Ho and Sm metals, respectively, and in these phases both the Ho and Pr sites are found to be fully ordered. However, T_N decreases more rapidly with decreasing x than is predicted using mean-field theory. No magnetic ordering is detected in the dhcp alloys, suggesting that Ho has a nonmagnetic singlet ground state. Furthermore, the ordering in Pr induced by the hyperfine interaction is suppressed by dilution with Ho.

ACKNOWLEDGMENTS

We would like to express our gratitude to R. A. Cowley and J. Jensen for help and advice and to thank J. Lebech of Risø National Laboratory and S. Pujol of the Institut Laue-Langevin for their expert technical assistance. Financial support was provided by the EPSRC in the United Kingdom and by the EU under its Large Scale Facilities Program in Denmark.

*Author to whom correspondence should be addressed.

FAX: 44-1865-272400.

Electronic address: GOFF@PHYSICS.OXFORD.AC.UK

[1] W. C. Koehler, J. W. Cable, M. K. Wilkinson, and E. O. Wollan, Phys. Rev. **151**, 414 (1966).

[2] D. Gibbs, D. E. Moncton, K. L. D'Amico, J. Bohr, and B. H. Grier, Phys. Rev. Lett. **55**, 234 (1985).

[3] R. A. Cowley and S. E. Bates, J. Phys. C **21**, 4113 (1988).

[4] H. Bjerrum Møller, J. Z. Jensen, M. Wulff, A. R. Mackintosh, O. D. Masters, and K. Gschneidner, Phys. Rev. Lett. **49**, 482 (1982).

[5] J. Jensen and A. R. Mackintosh, *Rare Earth Magnetism* (Oxford

University Press, Oxford, 1991).
[6] K. A. McEwen, W. G. Stirling, and C. Vettier, Phys. Rev. Lett. **41**, 343 (1978).
[7] K. A. McEwen, G. J. Cock, L. W. Roeland, and A. R. Mackintosh, Phys. Rev. Lett. **30**, 287 (1973).
[8] H. R. Child, W. C. Koehler, E. O. Wollan, and J. W. Cable, Phys. Rev. A **138**, 1655 (1965).
[9] W. C. Koehler, in *Magnetic Properties of Rare Earth Metals*, edited by R. J. Elliott (Plenum, London, 1972), p. 81.
[10] R. A. Cowley, R. C. C. Ward, M. R. Wells, M. Matsuda, and B. Sternlieb, J. Phys.: Condens. Matter **6**, 2985 (1994).
[11] P. P. Swaddling, R. A. Cowley, R. C. C. Ward, M. R. Wells, and D. F. McMorrow, Phys. Rev. B **53**, 6488 (1996).
[12] C. Bryn-Jacobsen, R. A. Cowley, D. F. McMorrow, J. P. Goff, R. C. C. Ward, and M. R. Wells, Phys. Rev. B **55**, 317 (1997).
[13] K. A. McEwen, B. Lebech, and D. Fort, J. Magn. Magn. Mater. **54-57**, 457 (1986).
[14] S. W. Zochowski, W. G. Marshall, K. A. McEwen, E. M. Fawcett, E. M. Forgan, D. Fort, and S. Shaik, Physica B **180-181**, 26 (1992).
[15] J. Wolny and B. Lebech, J. Magn. Magn. Mater. **140-144**, 741 (1995).
[16] A. Vigliante, M. J. Christensen, J. P. Hill, G. Helgesen, S. Aa. Sørensen, D. F. McMorrow, Doon Gibbs, R. C. C. Ward, and M. R. Wells, following paper, Phys. Rev. B **57**, 5941 (1998).
[17] W. C. Koehler and R. M. Moon, Phys. Rev. Lett. **29**, 1468 (1972).
[18] A. J. Freeman, in *Magnetic Properties of Rare Earth Metals* (Ref. 9), p. 245.
[19] N. Achiwa and S. Kawano, J. Phys. Soc. Jpn. **35**, 303 (1973).
[20] B. D. Rainford, L. Cussen, J. Jensen, and D. Fort, J. Magn. Magn. Mater. **76-77**, 399 (1988).
[21] J. Jensen (private communication).
[22] C. C. Larsen, J. Jensen, and A. R. Mackintosh, Phys. Rev. Lett. **59**, 712 (1987).
[23] J. G. Houmann, B. D. Rainford, J. Jensen, and A. R. Mackintosh, Phys. Rev. B **20**, 1105 (1979).
[24] A. V. Andrianov, J. Magn. Magn. Mater. **140-144**, 749 (1995).
[25] R. J. Elliott and F. A. Wedgwood, Proc. Phys. Soc. London **84**, 63 (1964).